Research Article | Vol. 30, No. 21 / 10 Oct 2022 / Optics Express 37536
Optics EXPRESS

Subaquatic indirect laser ablation technique for glass processing

Ana I. Gómez-Varela,[1,*] Raúl Sanchez,[1] Bastián Carnero,[1,2] Luis Diaz-Gomez,[3] M. Teresa Flores-Arias,[1] and Carmen Bao-Varela[1,4]

[1]Photonics4Life Research Group, Departamento de Física Aplicada, Facultade de Física and Facultade de Óptica e Optometría, Instituto de Materiais (iMATUS), Universidade de Santiago de Compostela, Campus Vida, E15782 Santiago de Compostela, Spain
[2]BFlow S.L., Edificio Emprendia, Santiago de Compostela, Spain
[3]Departamento de Farmacología, Farmacia y Tecnología Farmacéutica, I+D Farma (GI-1645), Facultad de Farmacia, Instituto de Materiais (iMATUS) and Health Research Institute of Santiago de Compostela (IDIS), Universidade de Santiago de Compostela, E15782 Santiago de Compostela, Spain
[4]carmen.bao@usc.es
[*]anaisabel.gomez@usc.es

Abstract: Subaquatic indirect Laser-Induced Plasma-Assisted Ablation (SLIPAA) is proposed as a laser-based technique for glass processing. In this configuration, a water layer is added between a metallic target and a soda-lime glass substrate, so the processing of the glass is due to a combination of the ablation mechanism, the shock waves, and the cavitation bubbles. Thus, this method makes it possible to produce higher depth structures than those performed up to now by other standard laser techniques based on ablation, achieving structures in glass with rectangular cross-sectional profiles. Channels of 1 mm width are fabricated, reaching an average maximal depth value of almost 1400 µm at 30 passes of the laser beam while keeping the focal position fixed. Furthermore, the difference between processing the material with and without the addition of the water layer is presented. The influence of the processing parameters on the shape and quality of the fabricated structures is studied by optical and confocal microscopy, microcomputed tomography, and scanning electron microscopy. Compositional analysis of the glass is performed by energy dispersive X-ray technique to assess the transference of material from the metallic target to the fabricated channels. Deeper and more complex structures are obtained by refocusing the laser beam on the target and adding a pulsed flowing water film.

1. Introduction

On 18th May 2021 the United Nations General Council approved a resolution declaring 2022 the International Year of Glass [1]. This resolution directs political and public attention to the importance of glass in various sectors of the society, arranging from the aerospace and automotive industries to healthcare, architecture, and basic researching in a multitude of disciplines (biology, physics, chemistry and so on). Glass substrates play a very important role in different researching and industrial fields due to its unique combination of excellent mechanical, thermal, electrical, chemical, and optical properties. It has been used for fabricating everything from optical waveguides for photonics circuits [2,3] to high efficiency diffraction gratings for telecommunication systems [4] or Lab-On-a-Chip systems for biological and biomedical applications [5,6].

A wide variety of glasses with different characteristics suitable for specific applications is currently available in the world market. At the same time, considering these characteristics and the desired results to be achieved, different technologies for glass processing and machining have been developed. A great number of micromachining glass technologies has emerged in the last

#463803 https://doi.org/10.1364/OE.463803
Journal © 2022 Received 19 May 2022; revised 21 Jul 2022; accepted 28 Jul 2022; published 26 Sep 2022

Optics EXPRESS

decades that allow complex structures to be created by combining channels, holes, pillars and wells, for instance [7,8]. One of the most promising glass processing techniques is the laser processing, mainly because it is a single-stage process that is very flexible, low-polluting and fast enough to be suitable for mass production. In laser processing, long-pulse and short-pulse lasers can be used depending on the quality required in the process, the amount of material to be removed and the affordable cost. Although focusing a laser directly on the glass is an efficient strategy for machining glass, it is not the only possible way to do so. Normally, glass absorbs very small amounts of ultraviolet, visible, and infrared light, so an increasing of energy is needed to start the mechanizing of the glass, which often results in the generation of damage such as fractures and cracks on its surface. Infrared (IR) lasers are one the most implemented at the industry, so, it is necessary to develop new techniques to increase the IR absorption and thus improve the machining results. Some of the authors have devoted their efforts to this end, and have evaluated the role of the impurities in the absorption of the laser energy to initiate the ablative process [9]. There are other techniques that include: laser etching by self-regulating absorbing layer (LESAL) [10], laser-induced back side dry etching (LIBDE) [11] and laser-induced back side wet etching (LIBWE) [12]. However, the implementation of these techniques is not simple because they require either a reactive gas in which to immerse the sample or a good deposition of the thin film on the surface of the glass that will be subsequently removed by chemical etching. Other studies focused on laser cutting methods of soda-lime glass in air and assisted by water with picosecond and nanosecond lasers have been recently reported by Dudutis et al., emphasising the importance of understanding and developing emerging glass processing techniques [13]. In 1998, Zhang et al. [14] proposed a novel technique for high-speed machining of glass called laser-induced plasma-assisted ablation (LIPAA), which allowed the use of nanosecond UV and visible lasers for micromachining of materials that were transparent at these wavelengths. This opens the door to a new simple and fabrication method available in many laboratories that permits surface microstructuring, colour marking [15], painting and selective metallization of glass [16] as well as microchannels surface fabrication for microfluidic and biological studies [7].

In the last years, milli and microfluidics are emerging as fields of great interest due to their multiple applications in chemistry, engineering, and medicine, among others. Both milli and microfluidic devices can have very complex structures, where the channel can be considered as the fundamental unit. By means of laser ablation it is possible to make channels and microchannels with varied dimensions and geometries on glass substrates. Additionally, glass shows the advantage of high casting lifetime and can also be used to perform masters that could be replicated by biocompatible polymers such as Polydimethylsiloxane (PDMS) for biological applications [17]. Taking advantage of the impurities of the glass it is possible to manufacture structures by laser ablation, even for substrates that are transparent to the laser wavelength [9]. However, the dimensions of such structures are in the order of tens of micrometers. To manufacture structures of larger size (millimeter-sized channels), the most suitable technique is LIPAA. This technique consists on focusing a laser onto a metallic target located under a glass or a material transparent to the wavelength of the laser used [18–20]. The plasma generated by the interaction of the laser with the metallic target allows to initiate the ablation of the back face of the glass. Using this technique, structures with dimensions of millimeters that mimic large blood vessels have been manufactured, in particular, bifurcations of vessels coronary arteries [17].

The Under Liquid Laser Beam Machining (UL-LBM) technique consists of facilitating the ejection of the processed material in the presence of a liquid. During the UL-LBM process, thermal loading and redeposition of material debris in the work area are reduced because the specific heat capacity of the liquid and thermal conductivity are higher than that of air. Additionally, the extracted material is prevented from solidifying on the substrate [21]. Liquid immersion shows advantages such as increased plasma-induced recoil pressure due to water confinement and the collapse of cavitation bubbles [22]. The plasma generated in the ablation

Optics EXPRESS

process absorbs part of the incident laser energy and reduces the coupling of the laser energy with the material surface giving rise to what is known as the shielding effect. The incorporation of the liquid causes both the size and duration of the plasma to be reduced. The delay in the onset of plasma formation causes the overlap with the laser pulse to decrease [23], weakening the plasma shielding effect and improving the efficiency of the process. Recently, Song et al. [24] obtained images of the shock wave and cavitation bubble generation process in laser-processed metallic targets under water, observing a temporal overlap of both processes, which are fundamental results to understand the laser ablation processes under water. In this regard, direct laser ablation of soda-lime glass sheets in ambient air and water-assisted conditions using a picosecond laser operating at 532 nm was presented by Markauskas et al. [25]. Results showed that the application of a thin flowing water film on the sample's surface improved the glass ablation efficiency by 12 times. Water immersion was also proposed by An et al. [26] for reducing redeposition and blocking effect when drilling holes of micrometers on soda-lime glass by femtosecond laser pulses. Ten years later, Xu et al. presented the fabrication of glass microfluidic structures using water-assisted femtosecond-laser ablation followed by electroless plating [27]. The addition of water during the laser direct-writing ablation process enhances the removal of the debris generated inside the glass, improving the final quality of the ablated micropatterns. However, femtosecond systems are less present in the industry than nanosecond lasers, which have the following advantages over the former: low cost, compact size, robustness, minimal maintenance, lower exigences in the environment conditions and lower safety requirements. For instance, Gecys et al. [28] used a nanosecond laser working in air at 532 nm focused on the backside of the glass for achieving micro-holes with high aspect ratio.

Nevertheless, to the best of our knowledge, the precise manufacturing of glass with rectangular cross section, steep edges (vertically) and great depth is still a challenge for ablation techniques relying on nanosecond laser. The depth of the channels obtained by the mentioned methods is limited. To overcome this limitation in the depth of the channels, we have developed a technique that also reduces the thermal effects generated by the laser and moreover, it facilitates the ejection of material from the laser-plasma interaction zone. We name this technique SLIPAA (Subaquatic LIPAA). In this technique, a simple set-up is used. A laser beam, after passing through a glass substrate and a layer of deionized water, is focused onto a metal target piece. The laser source is a Nd:YVO_4 laser operating at its fundamental wavelength, 1064 nm, with a pulse duration of 20 ns and is combined with a galvanometer system and a flat field lens that grants a homogeneous energy distribution on the target. When the laser is focused onto the metallic target, a plasma located between the glass substrate and the target, is generated and confined by the water layer. The thermal effects produced by the nanosecond laser beam are weakened and the expulsion of material from the laser plasma interaction zone is facilitated. The mechanical shock waves [29,30], generated by the focused laser, combined with the ablation plume and the cavitation bubbles generated in the process, perform the ablation on the rear face of the glass.

SLIPAA could be considered as a combination of LIPAA and LIBWE. Both ablation processes are perfectly described in [31,32] and [33,34], respectively. Nevertheless, recent analysis of under-liquid target ablation, such as [24], must also be considered to fully describe the SLIPAA process. In this work, Song et al. demonstrate the propagation of supersonic shock waves from the target to the water in the opposite direction to the impinging laser beam. At the beginning of the process, they observe that the shock wave in water is overlapped with the plasma and propagates into it with a planar front and at supersonic speed. After a few hundreds of nanoseconds, the plane wave changes into an ideal spherical wave. Few microseconds later new planar shock waves are generated. These secondary waves are associated to the elastic (or sound) wave propagating into the target that was plasma-induced. However, the mechanism to describe SLIPAA and how the ablation occur at the rear side of the glass is still not clearly understood and further studies

Optics EXPRESS

involving the laser-plasma interaction, shock waves propagation and interference, hydrodynamic behaviour of cavitation bubbles and heat exchange processes, must be carried out.

Compared to previous glass machining processes, SLIPAA presents some advantages such as simplicity and design flexibility, being capable of fabricating complex elements with more depth than other glass structuring techniques [16]. A variety of structures in the millimeter and micrometer range with vertical sidewalls can therefore be processed using a simple and versatile experimental set-up. The capabilities of SLIPAA are demonstrated here by the manufacturing of channels on glass substrates as the first step to fabricate more complex devices or circuits. The performance of a fluidic device strongly depends on the surface characteristics of the channel, therefore the ability to modify the surface is a crucial factor to optimize the overall device operation. As surface roughness can be modified in a controlled manner by post-thermal treatments [35], some of the samples have been further subjected to a heat treatment to evaluate the influence on the roughness. In addition, a comparison between channels fabricated by LIPAA and SLIPAA is also presented and analyzed. The samples are characterized by optical and confocal microscopy, SEM microscopy, EDX and microcomputed tomography to assess surface quality, depth, roughness, and transference of material from the metallic target to the fabricated structures.

The paper is structured as follows: section 2 introduces the proposed SLIPAA technique, and the set-up and materials used in the experiment. Section 3 shows the study conducted to determine the optimal processing parameters by SLIPAA by manufacturing rectangular channels. Additionally, a comparison with channels obtained by LIPAA in terms of achieved depth is presented. Last, the versatility of the technique is demonstrated by fabricating structures with other geometries. The main findings of the study are summarized in section 4.

2. Materials and methods

Materials. The glass substrate employed is a low-cost float soda-lime glass of 5 mm width acquired from a local supplier. It presents low absorbance at 1064 nm, the center wavelength of the laser system, so it is suitable for the fabrication of the elements shown in this research.

The metallic sheets used as targets to generate the ablation plume are known as "Hardened Spring Steel W.-Nr. 1.1274" (H + S Präzisionsfolien GmbH, Pirk, Germany), with a carbon content of over 1%. Glass substrates were cleaned with detergent, washed in running water and then cleaned with isopropyl alcohol (IPA) in an ultrasonic cleaner for 30 min. Metallic targets were thoroughly rinsed with IPA.

Fabrication method and set-up. SLIPAA experiments on soda-lime commercial glass substrates were carried out using the set-up depicted in Fig. 1. A Q-Switched Nd:YVO_4 laser (Rofin; Plymouth, MI, USA) operating at 1064 nm and pulse duration of 20 ns is combined with a galvanometer system for steering the output laser beam. Nominal beam diameter is 20 µm. A flat-field lens of focal length of 160 mm provides a uniform irradiance distribution on the glass substrate over a working area of 120×120 mm^2. The beam is focused onto a metallic target after it passes through the glass substrate, which presents low absorption in the infrared region where the laser operates. There is a layer of deionized water of 145 µm thickness between the glass substrate and the metal target.

Thermal treatment. After the SLIPAA processing of the samples, a thermal treatment is applied using a LKN 86 furnace (Nannetti S.R.L., Faenza RA, Italia), with the aim of modifying, in a controlled manner, the surface roughness produced by the ablation on the bottom of the samples. The furnace has a temperature ramp function that allows to control the initial, process and final temperature of the samples, as well as the time of temperature exposure.

Sample analysis. The topography and surface roughness of the fabricated samples were characterized by confocal microscopy technique using a 3D optical profilometer S neox (Sensofar Metrology, Terrassa, Spain). The superficial quality at the edges of the structures were

Optics EXPRESS

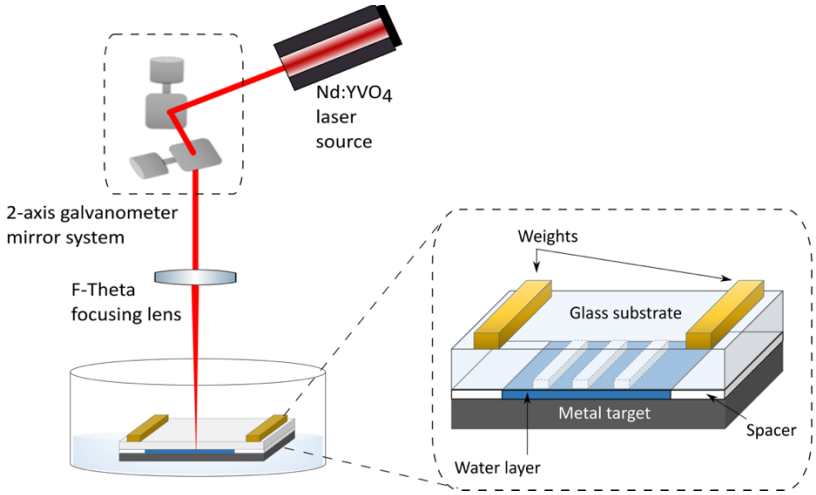

Fig. 1. Experimental set-up implemented for SLIPAA method. (a) Schematic representation of the experimental set-up, where a galvanometric mirror system steers the laser beam that goes through the substrate and the water layer, being focused on the metal target with a flat-field lens. (b) Detail of the set-up on the sample region: the glass substrate is separated from the metallic target using two spacers and two weights are used to ensure the glass is not shifted during the ablation process. All the elements are placed in a cuvette and filled with deionized water without fully covering the glass substrate.

also inspected by optical microcopy using a Nikon MM-400 metallurgic microscope (Nikon Instruments Europe B.V., Amsterdam, The Netherlands).

The samples were studied using an EVO LS 15 scanning electron microscope (Zeiss; Oberkochen, Germany). Compositional analysis was performed by Energy Dispersive X-Ray (EDX) technique to determine the possible transference of material from the metallic target to the fabricated channels. Data was acquired at 20 kV.

Furthermore, samples were also evaluated by microcomputed tomography (μCT) using a SkyScan 1272 X-ray microCT (Bruker; Kontich, Belgium) with a resolution of 13 μm/pixel and a Cu 0.11 mm filter. The obtained projections were reconstructed using Nrecon software and the analysis of the structures was carried out with CTAn software (Bruker; Kontich, Belgium). The reconstructed images were volume-rendered using CTVox software (Bruker) to visualize the structures fabricated in the glass substrates.

Pictures of the actual experimental set-up are displayed in Fig. 2. The geometry of the structure to be engraved on the glass substrate is first designed using a CAD-like (computer-aided design) software. The laser beam is focused on the steel sheet and the ablation plume generated directs towards the backside of the glass substrate. It can be appreciated how part of the debris generated from the ablation of the glass has been swept along towards the edges of the substrate, an effect promoted by the addition of the water layer. In a common LIPAA process, glass debris typically accumulates and suffer a solidification below the substrate, preventing further removal of the material.

Optics EXPRESS

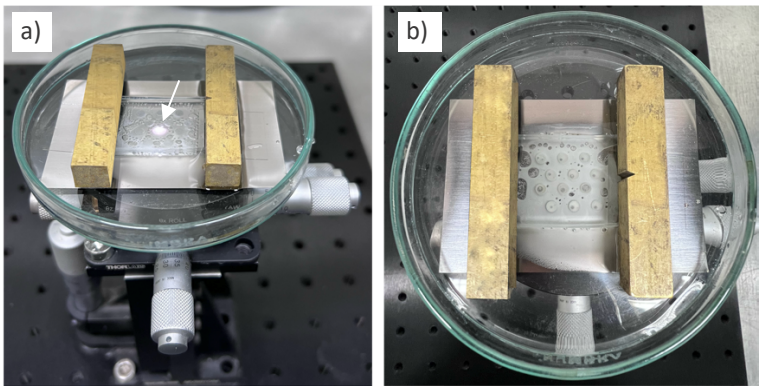

Fig. 2. Image of the set-up for glass processing using SLIPAA. (a) General view of the set-up during the laser operation. White arrow indicates the laser plasma generated on the metallic target. (b) Top view of the glass substrate once the process is finalized. The white debris corresponds to the material removed from the substrate. Some of the bubbles generated during the process can also be observed in the picture.

3. Results and discussion

3.1. Selection of the processing parameters

The laser system used in this set-up allows different processing parameters to be varied, such as average power, repetition rate and beam scanning velocity. Therefore, as a first step for the fabrication process, a study of proper laser parameters must be carried out. Hence, different combinations of these processing parameters have been analyzed to demonstrate the capabilities of SLIPAA for glass structuring. First, the effect of the laser repetition rate on rectangular cross-sectional channels depth was evaluated. The intensity delivered to the laser diode pumps, which is related to the laser average power, was fixed at 32 A (corresponding to 4.92 W average power at a repetition rate of 10 kHz) throughout the experiments. As it will be discussed in more detail later, several laser passes have been performed to obtain good rectangular channel geometries. Scanning speed was set to 200 mm/s due to a notably decrease of defects in the edges of the channels (such as cracks and irregular edges). These results are shown in Fig. 3, where optical microscope images of channels of 1 mm width fabricated with scanning velocities ranging from 100 to 1000 mm/s are shown. It is clearly exposed the influence of the laser scanning speed on the superficial damage around the edges of the channel. Significant crack formation along the scribe channel is observed below and above 200 mm/s laser beam velocity, while the better-quality edges are obtained for a scan speed of 200 mm/s. We attribute the surface damage in the structures at higher deflection velocities to the propagation of the shock waves, while at velocities below 200 mm/s thermal effects due to overlapping of the pulses combined with the shock waves are the responsible of the glass cracks. At 200 mm/s, for the processing parameters optimized in our experiments, it seems that the combination of these effects produces minimum damage on the glass surface. Further research on the combination of these effects remains to be performed.

Figure 4 shows that the depth of the channels obtained decreases with the laser repetition rate. It is worth mentioning here that the quality of the edges of the channels was found to strongly depend on this parameter, and the number of cracks and irregularities increases notably for values above 10 kHz. It can also be observed from the results presented in the figure that the reproducibility of the channels depth decreases significantly for higher repetition rates.

Optics EXPRESS

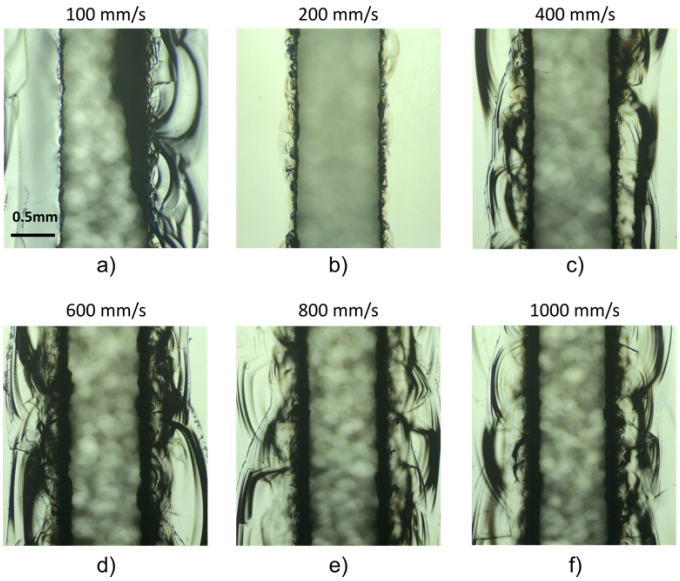

Fig. 3. Optical microscope images of channels of 1 mm width fabricated using the following scan speeds: (a) 100 mm/s, (b) 200 mm/s, (c) 400 mm/s, (d) 600 mm/s, (e) 800 mm/s, and (f) 1000 mm/s. Processing parameters: wavelength 1064 nm, 10 kHz repetition rate, fluence 78.3 J/cm^2, 30 laser passes. The scale is the same in all pictures.

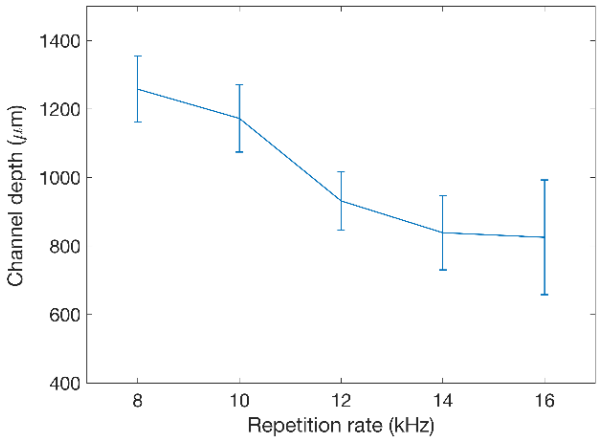

Fig. 4. Evolution of the mean depth value of the channels with the laser repetition rate. Processing parameters: wavelength 1064 nm, speed 200 mm/s and 30 laser passes. Error bars represent the standard deviation (N = 10).

Optics EXPRESS

The effect of the number of laser scans on the shape and depth of the channels is also evaluated. To obtain deep channels in glass substrates, several laser passes are needed. Moreover, this parameter influences the shape of the profile of the channels. A repetition rate of 10 kHz is set throughout the next experiments, observing a threshold on the number of laser passes necessary to achieve rectangular shaped channels, while keeping the laser focal distance fixed. Figure 5 shows the profile of three representative channels fabricated with the same laser processing parameters but with 2, 5 and 10 passes of the laser beam. From this figure it follows that below 10 laser scans channels with sloping walls are obtained, while from 10 laser passes onwards channels with vertical sidewalls are achieved. Also, the depth of the channels increases with the number of laser passes.

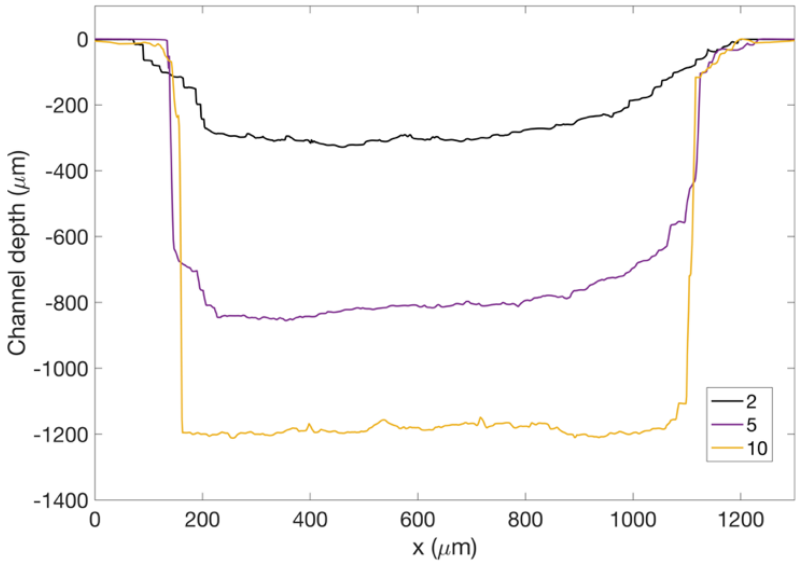

Fig. 5. Cross-sectional profiles of the channels with 2 (black line), 5 (purple line), and 10 (yellow line) laser passes. Well-formed channels with vertical sidewalls are obtained from 10 laser passes. Laser processing parameters: wavelength 1064 nm, 10 kHz repetition rate, fluence 78.3 J/cm^2, beam scanning speed 200 mm/s.

Channels have been fabricated increasing the number of laser passes from 10 up to 50, in steps of 10. The maximal depth is achieved at 30 laser passes with a mean depth value of 1385.56 μm. Above 30 laser passes, the depth of the channels diminishes, probably due to the accumulation of ablated material. In this case, it would seem that water movement and cavitation bubbles are not able to remove the debris produced in the ablative process out of the channel, so solidification of some of the material at the bottom of the channel may occur. A confocal 3D reconstructed image and the extracted profile of the channel obtained after 30 laser passes showing the vertical walls attained with SLIPAA are shown in Fig. 6(a) and Fig. 6(b), respectively. The dependence of the depth of the channels on the number of passes of the laser is shown further on in section 3.2, where a comparison between SLIPAA and LIPAA is presented (Fig. 7). Regarding the minimum achievable width, unobstructed good-quality channels of 300 μm width and around 1.36 mm depth, i.e. aspect ratio (the ratio of depth to width) of 4.53, have been obtained. The laser processing parameters are those of Fig. 5, with 30 laser passes and fixed focus position.

Roughness is another critical parameter to decide the quality of the structured surface in different applications. Surface roughness affects the wettability of liquid over a solid surface, which generally increases when decreasing the surface roughness. This, for instance, is important in experiences involving flows in fluidic experiments, where the fluid flow pattern is sensitive to

Optics EXPRESS

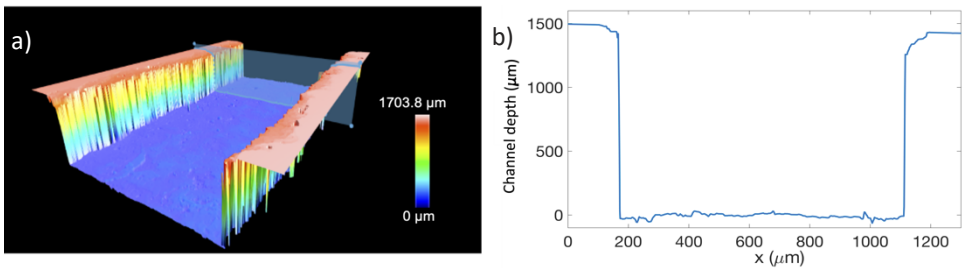

Fig. 6. (a) Confocal 3D reconstructed micrograph for surface topography analysis of one representative rectangular channel, and (b) corresponding cross-sectional profile. Processing parameters: wavelength 1064 nm, 10 kHz repetition rate, fluence 78.3 J/cm^2, beam scanning speed 200 mm/s and 30 laser passes.

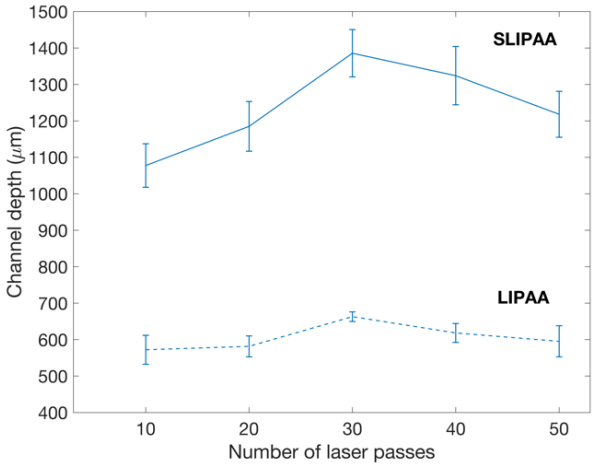

Fig. 7. Comparison of the evolution of the depth of the channels with the number of laser passes with SLIPAA (solid line) and LIPAA (dashed line). Laser processing parameters: wavelength 1064 nm, 10 kHz repetition rate, fluence 78.3 J/cm^2, beam scanning speed 200 mm/s. Error bars represent the standard deviation (N = 10).

many intrinsic parameters such as surface roughness [36]. Physical modification of the channels surface features is also relevant for cellular attachment in bioassays [37,38], where cell attachment level might vary depending on the cell types. Another example can be found in the interaction of the fluids with light from embedded optical waveguides in optofluidic chips and lab-on-a-chip devices [39], where the fabrication parameters must be optimized to minimize the microchannel roughness.

The surface roughness at the bottom of those channels presented in Fig. 4 is studied as function of the laser repetition ration rate. Roughness was determined using the arithmetical mean height (Sa), obtained from confocal microscopy measurements along the bottom of the channels over a defined area of 250×250 µm^2. The corresponding values are shown in Table 1, where the surface roughness is measured to be between 12.18 µm and 19.19 µm.

Surface roughness as function of the number of laser passes is presented in Table 2. Sa reaches a maximum value at 30 laser passes, while it is minimum at 50 laser passes. This effect can be attributed to the fact that after 30 laser passes the ablation efficiency of the process decreases with more accumulation of the debris under the channels and the subsequent solidification of part of this material on the surface of the channels.

Optics EXPRESS

Table 1. Arithmetical mean height values corresponding to the roughness of the bottom of the channels presented in Fig. 4.[a]

Rep. rate (kHz)	8	10	12	14	16
Sa (µm)	12.18 ± 3.34	13.75 ± 4.28	15.29 ± 3.81	15.01 ± 4.51	19.10 ± 5.24

[a]Measurements were performed according to the ISO 25178 standard. Number of samples for statistical analysis is N = 10.

Table 2. Roughness of the channels as function of the number of laser passes.[a]

Number of laser passes	10	20	30	40	50
Sa (µm)	13.75 ± 4.28	12.91 ± 2.58	14.77 ± 3.11	11.72 ± 2.42	11.05 ± 1.19

[a]Arithmetical mean height values correspond to the structures presented in Fig. 7 fabricated by SLIPAA. Measurements were performed according to the ISO 25178 standard. Number of samples for statistical analysis is N = 10.

The combination of SLIPAA technique with a post-thermal treatment allows to improve the optical quality of the glass structures and the reduction of the initial roughness on the bottom of the channels. Hence, following the SLIPAA fabrication process, the channels were heated over the glass transition temperature for a pre-determined amount of time. In particular and considering that the glass transition temperature for soda-lime glass is 570°C, the effect on the roughness of the bottom of the channels for a post-thermal treatment of 590 °C to 630 °C in steps of 10 °C was evaluated. Each sample was pre-heated for 30 minutes from room temperature until the treatment temperature was achieved. This treatment temperature was maintained for 2 hours, allowing the melting of the material and its redistribution inside the channel. The influence of the post-thermal treatment on the superficial roughness reduction of the channels is listed in Table 3. We observe that for treatment temperatures from 590 °C to 620 °C, roughness decreases without affecting significantly feature dimensions, i.e., the structures maintain an almost rectangular cross-sectional profile in all cases. At 630 °C the profile of the channel is reshaped into a concave-like profile.

Table 3. Roughness reduction in the bottom of channels manufactured at 30 laser passes with the laser processing parameters of Fig. 6.[a]

Temperature (°C)	Roughness reduction (%)
590	26.21 ± 0.56
600	30.14 ± 0.79
610	32.15 ± 0.99
620	39.47 ± 0.43
630	63.19 ± 0.44

[a]Measurements were performed according to the ISO 25178 standard.

3.2. Channel fabrication with SLIPAA and LIPAA processes: a comparison

In order to visualize the potential of SLIPAA for glass processing, we compare the results with those obtained for channels fabricated with LIPAA. Figure 7 shows the evolution of the depth of the channels fabricated via laser-induced plasma-assisted ablation in air (dashed line) and subaquatic laser-induced plasma-assisted ablation (solid line). We use the set-up described in section 2 with the exception that there is no water layer between the metallic target and the

Optics EXPRESS

glass, i.e. the substrate and the target are separated by air. Therefore, 1 mm width channels are fabricated on glass for a number of laser scans from 10 to 50. A similar trend is observed in this case, where again a maximum channel depth is reached for 30 laser scans. However, there is a significant difference in the depth reached by SLIPAA and LIPAA. While for the former the maximum average depth reached is 1385.56 µm, only 662.92 µm is reached with the latter.

To further picture the differences observed between both techniques, Fig. 8 shows microCT images of rectangular channels fabricated with a) 30 and b) 50 laser passes in air (LIPAA) and c) 30 and d) 50 laser passes in water (SLIPAA) from Fig. 7. Figure 8 images (a) and (b) reveal that when LIPAA is carried out, smaller aspect-ratio structures are obtained. Furthermore, a higher number of laser passes entails that the material expelled during the ablation is not able to evacuate the channel, which results in an inclined area at the bottom of the channel. On the contrary, with SLIPAA one can achieve channels with higher aspect-ratio for the same number of laser passes. Moreover, the bottom of the channel continues to be flat when the number of laser passes rises from 30 to 50.

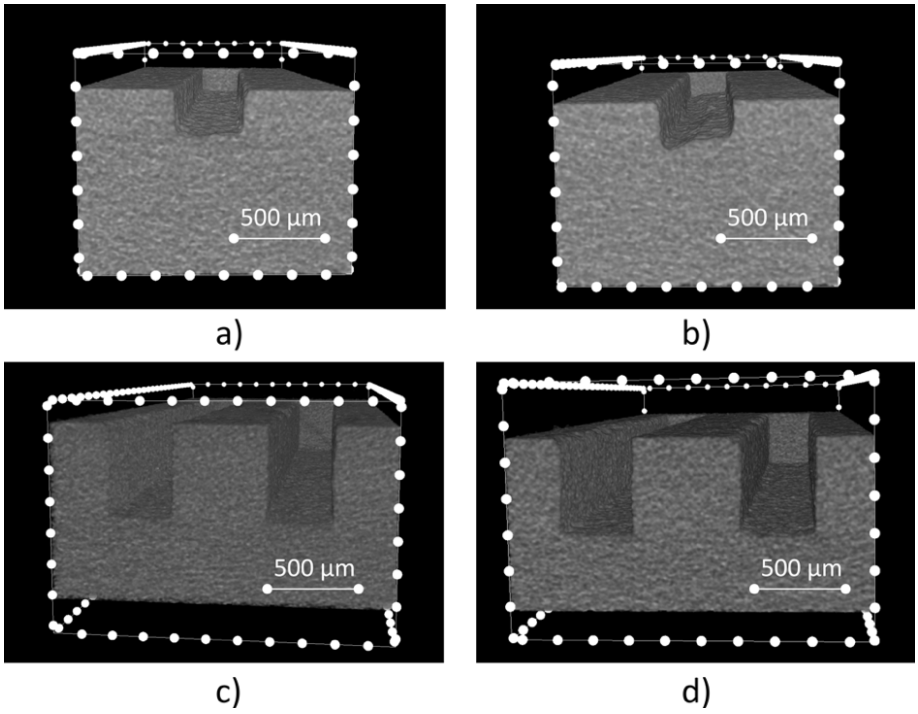

Fig. 8. MicroCT images of representative rectangular shaped channels fabricated with (a) 30 and (b) 50 laser passes in air (LIPAA) and (c) 30 and (d) 50 laser passes in water (SLIPAA). Scale denotes the distance between two consecutive points in the 3D image.

The cross section of rectangular shaped channels fabricated with SLIPAA for 30 and 50 laser scans are shown in Fig. 9. As discussed above, deeper structures are obtained for 30 laser passes (Fig. 9(a)). For a higher number of passes we observe that channel depth decreases, as shown in Fig. 9(b). In this case, the bottom of the channels is more uniform for 50 laser passes given the redeposition of the ablated material.

The surface of the bottom of channels manufactured by SLIPAA and LIPAA after 30 and 50 laser passes is inspected by SEM analysis in Fig. 10 and Fig. 11, respectively. In both cases a more homogeneous surface along the channel is obtained with SLIPAA. Moreover, laser ablation through the water film produced less redeposited debris, as can be seen in the figures. The debris

Optics EXPRESS

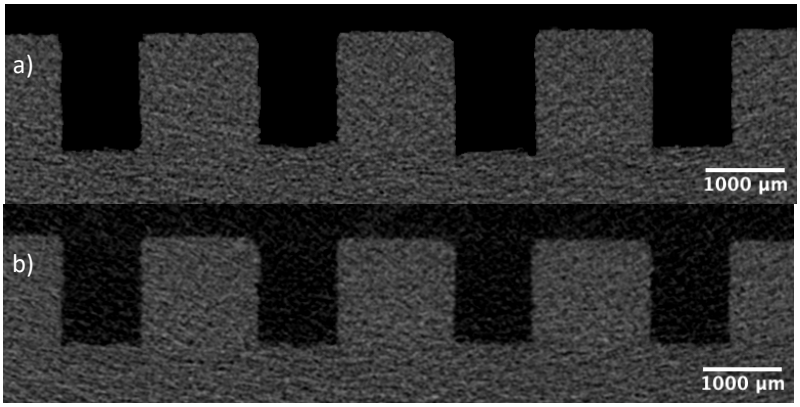

Fig. 9. Cross section of representative channels engraved on the glass substrates using SLIPAA after 30 and 50 laser passes are shown in (a) and (b), respectively. More homogeneous surfaces are obtained for 50 laser passes.

is even more abundant after 50 laser passes in air (Fig. 11(d)), while no significant traces of residues can be detected when the ablation is carried out in water (Fig. 11(b)). There is also less evidence of debris on the substrate along the edges of the channel when using SLIPAA compared to the manufacture of the channels with LIPAA, a fact illustrated in Fig. 10(c) and Fig. 11(c).

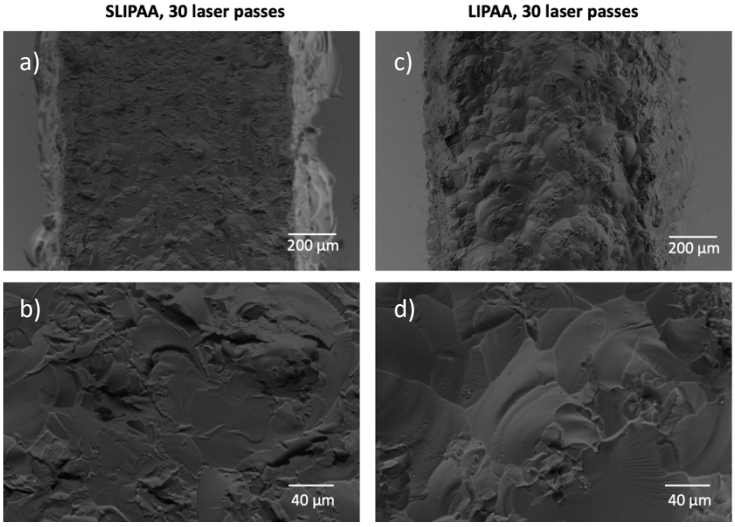

Fig. 10. SEM images of representative channel surfaces after 30 laser passes with SLIPAA (left) and LIPAA (right).

An analysis of the chemical composition of the structures fabricated by SLIPAA and LIPAA has been made by EDX. Different areas of the glass and the target before and after both fabrication processes have been evaluated. Figure 12 shows the EDX results obtained for a channel fabricated after 30 laser passes by SLIPAA and LIPAA. In both cases, the chemical composition on the bottom surface of the channel has been analyzed as well as on the glass surface out of the channel. The differences found in the chemical composition of the four analyzed zones in comparison with the untreated glass are highlighted in red. In the channel fabricated by SLIPAA (Fig. 12(a)), at the bottom of the channel and on the surface of the glass traces of C are detected as consequence

Optics EXPRESS

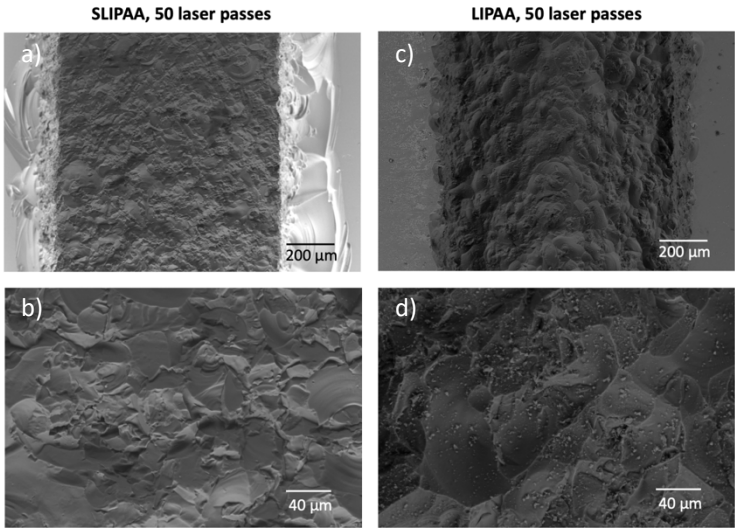

Fig. 11. SEM images acquired at the surface of the bottom of representative channels after 50 laser passes with SLIPAA (left) and LIPAA (right).

of the metal layer laser ablation. Nevertheless, N is only detected at the bottom of the channel. Note that in Fig. 12(b), corresponding to the channel fabricated by LIPAA, the untreated glass surface composition is not the same as that given in Fig. 12 (Fig. 12(a)). This is because the structures have been fabricated on different sides of the glass. During the fabrication process of the soda-lime glass, the molten glass is floated over a film of molten tin for obtaining a plane sheet glass with uniform thickness. Tin is transferred to the side of the glass in contact with the metal bath during this process, as the EDX analysis reveals. On the other hand, it is well known that tin impurities play a key role in direct laser glass micromachining process, but the effects of its presence are negligible in the case of glass processing by indirect methods such as SLIPAA or LIPAA. The chemical surface composition at the bottom of the channel fabricated by LIPAA reveals traces of C, S, K, Cr and Fe from the metal target, as well as the glass surface near the channel where C, K and Fe are also detected as consequence of ablation debris deposition. As a summary, for the channels fabricated by both methods, SLIPAA and LIPAA, transference from the metallic target to the channels surface is obtained, however this transfer is much less significant in the case of SLIPAA. The same trend was observed for the samples fabricated with 50 laser passes.

3.3. Versatility of the SLIPAA technique

In this work, we have presented a new water-assisted laser method for processing glass using a nanosecond laser. Channels of 1 mm width with vertical sidewalls and maximal mean depth value close to 1400 µm were fabricated after 30 laser passes. However, these structures were obtained without refocusing the laser during the whole fabrication process in order to study the capabilities of the SLIPAA process in its most simple configuration. But a significant issue during subaquatic LIPAA arises from the blocking of the laser beam provoked by the generation of debris during the ablation and the redistribution of material caused by bubbles. Nevertheless, the underwater laser ablation process can be enhanced by controlling both the water flow rate and the flow direction [40,41]. When combined with the readjustment of the focus on the metallic target, a better performance of the whole SLIPAA process can be achieved in order to fabricate deeper channels with less material redeposition.

Optics EXPRESS

a)

	Spectrum 4 Wt (%)
C	5.1
O	44.2
Na	8.6
Mg	1.3
Al	0.2
Si	33.5
Ca	7

Spectrum Label	Spectrum 1 Wt (%)	Spectrum 2 Wt (%)	Spectrum 3 Wt (%)
C	9.27	9.00	9.18
N	1.11	1.58	1.50
O	48.17	48.54	48.42
Na	8.39	8.45	8.47
Mg	1.14	1.07	1.16
Al	0.20	0.20	0.22
Si	26.26	25.83	25.81
Ca	5.46	5.33	5.24

	Untreated glass substrate Wt (%)
C	3.7
O	45.5
Na	9.0
Mg	2.4
Al	0.6
Si	33.2
Ca	5.5

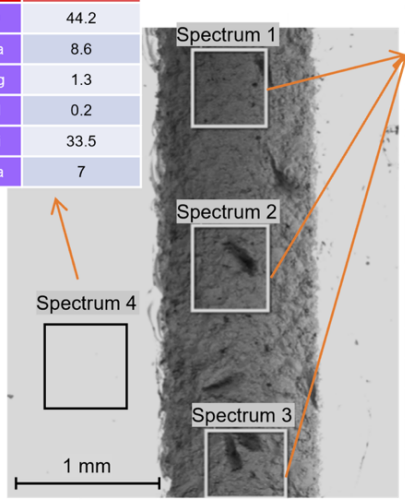

b)

	Spectrum 4 Wt (%)
C	3.9
O	44.3
Na	9.1
Mg	2.4
Al	0.6
Si	31.5
K	0.2
Ca	5.6
Fe	0.2
Sn	2.4

Spectrum Label	Spectrum 1 Wt (%)	Spectrum 2 Wt (%)	Spectrum 3 Wt (%)
C	7.58	7.21	5.53
O	48.17	47.82	47.65
Na	9.00	8.97	9.16
Mg	2.25	2.29	2.31
Al	0.50	0.52	0.51
Si	26.98	27.69	28.72
S		0.10	0.11
K	0.15		0.16
Ca	4.80	5.11	5.26
Cr			0.06
Fe	0.08	0.09	
Sn	0.49	0.20	0.52

	Untreated glass substrate Wt (%)
C	3.6
O	44.4
Na	9.1
Mg	2.4
Al	0.49
Si	32.1
Ca	5.6
Sn	1.9

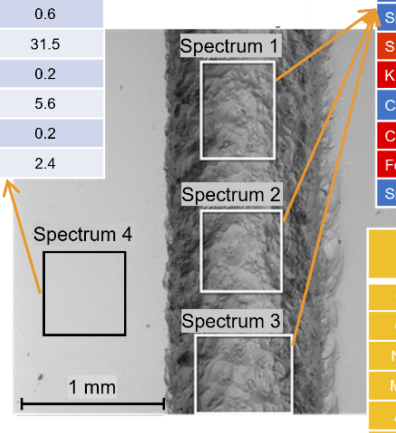

Fig. 12. EDX spectra of the channel surface fabricated by (a) SLIPAA and (b) LIPAA after 30 laser passes. The chemical analysis was determined in the bottom of the channel and on the glass substrate. The differences on the chemical composition between the processed area and the glass without treatment are highlighted in red.

Optics EXPRESS

Therefore, besides the tuning of the number of the laser passes and the laser processing parameters, the depth of the structures can be controlled by readjusting the focal spot position in the target and adding flowing water during the fabrication process. Additionally, this technique is not limited to the production of channels, but also allows for the fabrication of structures with different geometries. To exemplify the potential of the method's application, Fig. 13 shows wells of 3 mm in diameter generated into soda-lime glass substrates by SLIPAA. In Fig. 13(a) the top view of a 3×5 matrix of wells of 3 mm in diameter is shown, while in Fig. 13(b) a picture of wells ranging from 4.14 mm to 4.02 mm in depth is presented. A microCT image of an array of 1 mm depth wells is exhibited in Fig. 13(c). The set-up used is that described in section 2, with a nominal beam diameter of 20 µm. To manufacture the wells in Figs. 13(a) and 13(b), a water jet was carefully applied between the metallic target and the substrate every 5 laser passes. This stream of water washes away those debris previously generated during SLIPAA processing that could not be removed due to the water movement produced with the shock waves. In this step, special care must be taken to avoid unwanted displacement of the substrate and the generation of air bubbles that may be trapped inside the structures. The pulsed water flow was manually implemented. Additionally, the laser beam is refocused 40 µm on the metal foil every 10 laser passes to ensure that the ablation efficiency of the process is maintained. The processing time for each one of the wells shown in the figure is around 4 minutes.

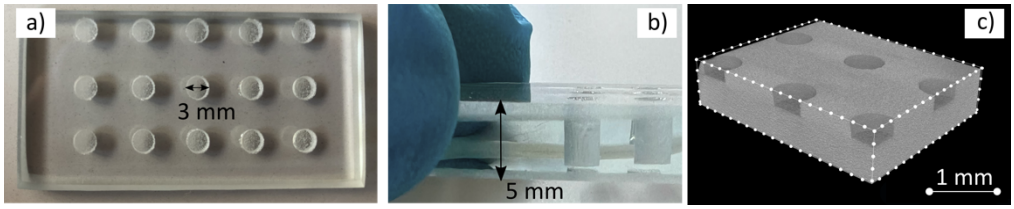

Fig. 13. Fabrication of wells with SLIPAA. (a) Top view of the 3×5 matrix of wells engraved inside a commercial soda-lime glass. (b) Image showing the depth of the wells where the maximal value achieved is over 4 mm. (c) MicroCT image of 1 mm deep wells with a diameter of 3 mm. A good agreement between the designed diameters in CAD and the fabricated wells is achieved. Processing parameters: wavelength 1064 nm, repetition rate 10 kHz, beam scanning speed 200 mm/s. In (a) and (b) the laser beam was refocused on the channel bottom surface to continue the ablation. The wells shown were obtained after 50 laser passes, where flowing water was used every 5 laser passes to carry away the debris generated during the process. In (c) the focal position was fixed during the manufacturing process. The scalebar denotes the distance between any two points in the 3D image.

Some uses of wells in fluidic and microfluidics platforms are, for instance, inlets, outlets, storage, and trapping components, among others. Besides channels and wells, other configurations defined by CAD design can be obtained by SLIPAA. Figure 14 shows a fluidic chip composed by 1 mm deep channels and wells.

Optics EXPRESS

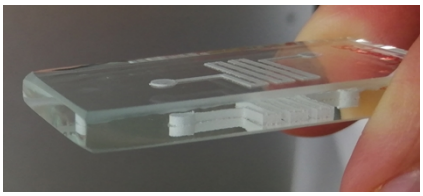

Fig. 14. Fluidic chip manufactured by SLIPAA. On the upper side of the glass one can see the reflected image of the chip. Processing parameters: wavelength 1064 nm, fluence 78.3 J/cm^2, repetition rate 10 kHz, beam scanning speed 200 mm/s, 10 laser passes.

4. Conclusions

A new technique using a nanosecond laser source for processing structures with different geometries in soda-lime glass substrates with dimensions in the millimeter range and vertical sidewalls is proposed. The technique consists of a subaquatic LIPAA process (SLIPAA), where the metallic target and the substrate are separated by a layer of water. This layer helps to confine the plasma generated over the target and to improve the material removal from the glass. The combination of the mechanical shock waves generated by the laser target irradiation, the plasma and the cavitation bubbles are responsible for the glass ablation. By this method, rectangular shaped channels with a variety of dimensions and excellent quality straight edges can be obtained when a minimum of 10 laser scans are applied. The highest depth mean value has been obtained for 30 laser passes, corresponding to 1385.56 µm, and achieving channels with vertical sidewalls. While the depth was found to decrease with the laser repetition rate, the roughness of the bottom of the channels increases with higher repetition rate. There is no upper limit on the width of the channels, which can be selected by varying the number of parallel laser scans. Regarding minimum achievable width, good-quality channels of 300 µm width and aspect ratio of 4.53 were manufactured. To demonstrate more clearly the potential of the technique, a comparative study between SLIPAA and LIPAA is also shown. In both cases, the depth of the structures increases with the number of laser repetitions, achieving its maximum value for 30 passes. However, a significant difference in mean channel depth is observed with LIPAA, where the highest value achieved is 662.92 µm. Moreover, EDX analysis on samples fabricated with SLIPAA and LIPAA revealed that transference of impurities from the metallic target to the channels surface is observed, however this transfer is much less significant in the case of SLIPAA. Moreover, SEM examination of the samples exposed less evidence of debris on both the bottom of the samples and the substrate along the edges of the channels when using SLIPAA compared to the manufacture of the structures with LIPAA. Deeper structures are obtained with multiple laser scans by incorporating a water flow and continuously readjusting the laser beam focus onto the metallic target. The technique presented here is not limited to the manufacturing of channels, allowing to obtain structures with different geometries overcoming the typical depth limitations of laser-fabricated structures on glass. In particular, wells of 4.14 mm deep were fabricated in 5 mm thick soda-lime substrates. Our findings indicate that SLIPAA can become an amazingly effective method in laser processing applications involving a large amount of material removal.

Funding. Agencia Estatal de Investigación, Ministerio de Economía y Competitividad (AEI RTI2018-097063-B-100); Consellería de Educación Xunta de Galicia/FEDER (ED431B 2020/29 UE); Consellería de Cultura, Educación e Ordenación Universitaria, Xunta de Galicia (ED481D-2021-019); Axencia Galega de Innovación (11_IN606D_2021_2604925).

Acknowledgments. Work supported by the Consellería de Educación Xunta de Galicia/FEDER (ED431B 2020/29 UE) and the Agencia Estatal de Investigación, Ministerio de Economía y Competitividad, Spain (AEI RTI2018-097063-B-100). Ana I. Gómez-Varela acknowledges Consellería de Cultura, Educación e Ordenación Universitaria for a Postdoctoral fellowship (Xunta de Galicia, Spain; ED481D-2021-019). B. Carnero thanks to GAIN/Xunta de Galicia by the contract under no. 11_IN606D_2021_2604925.

Optics EXPRESS

Disclosures. The authors declare no conflicts of interest.

Data availability. Data underlying the results presented in this paper are not publicly available at this time but may be obtained from the authors upon reasonable request.

References

1. UN General Assembly, "UN Resolution L84, International Year of Glass, 2022," https://undocs.org/en/A/75/L.84.
2. J.-E. Broquin and S. Honkanen, "Integrated Photonics on Glass: A Review of the Ion-Exchange Technology Achievements," Appl. Sci. **11**(10), 4472 (2021).
3. D. Tan, Z. Wang, B. Xu, and J. Qiu, "Photonic circuits written by femtosecond laser in glass: improved fabrication and recent progress in photonic devices," Adv. Photonics **3**(02), 024002 (2021).
4. N. Takeshima, Y. Narita, S. Tanaka, Y. Kuroiwa, and K. Hirao, "Fabrication of high-efficiency diffraction gratings in glass," Opt. Lett. **30**(4), 352 (2005).
5. F. Sima, K. Sugioka, R. M. Vázquez, R. Osellame, L. Kelemen, and P. Ormos, "Three-dimensional femtosecond laser processing for lab-on-a-chip applications," Nanophotonics **7**(3), 613–634 (2018).
6. K. L. Wlodarczyk, D. P. Hand, and M. M. Maroto-Valer, "Maskless, rapid manufacturing of glass microfluidic devices using a picosecond pulsed laser," Sci. Rep. **9**(1), 20215 (2019).
7. L. Hof and J. Abou Ziki, "Micro-Hole Drilling on Glass Substrates—A Review," Micromachines **8**(2), 53 (2017).
8. S. Schwarz, S. Rung, C. Esen, and R. Hellmann, "Ultrashort pulsed laser backside ablation of fused silica," Opt. Express **29**(15), 23477 (2021).
9. D. Nieto, J. Arines, and M. T. Flores-Arias, "Fluence ablation threshold dependence on tin impurities in commercial soda-lime glass," Appl. Opt. **53**(24), 5416 (2014).
10. R. Bohme and K. Zimmer, "Low roughness laser etching of fused silica using an adsorbed layer," Appl. Surf. Sci. **239**(1), 109–116 (2004).
11. B. Hopp, C. Vass, T. Smausz, and Z. Bor, "Production of submicrometre fused silica gratings using laser-induced backside dry etching technique," J. Phys. D: Appl. Phys. **39**(22), 4843–4847 (2006).
12. J. Wang, H. Niino, and A. Yabe, "One-step microfabrication of fused silica by laser ablation of an organic solution," Appl. Phys. A: Mater. Sci. Process. **68**(1), 111–113 (1999).
13. J. Dudutis, L. Zubauskas, E. Daknys, E. Markauskas, R. Gvozdaitė, G. Račiukaitis, and P. Gečys, "Quality and flexural strength of laser-cut glass: classical top-down ablation versus water-assisted and bottom-up machining," Opt. Express **30**(3), 4564 (2022).
14. J. Zhang, K. Sugioka, and K. Midorikawa, "High-speed machining of glass materials by laser-induced plasma-assisted ablation using a 532-nm laser," Appl. Phys. A: Mater. Sci. Process. **67**(4), 499–501 (1998).
15. Y. Hanada, K. Sugioka, I. Miyamoto, and K. Midorikawa, "Colour marking of transparent materials by laser-induced plasma-assisted ablation (LIPAA)," J. Phys.: Conf. Ser. **59**, 687–690 (2007).
16. K. Sugioka, K. Midorikawa, H. Yamaoka, Y. Gomi, M. Otsuki, M. H. Hong, D. J. Wu, L. L. Wong, and T. C. Chong, "Glass microprocessing by laser-induced plasma-assisted ablation: fundamental to industrial applications," Proc. SPIE **5506**, 1–10 (2004).
17. M. Aymerich, E. Álvarez, C. Bao-Varela, I. Moscoso, J. R. González-Juanatey, and M. T. Flores-Arias, "Laser technique for the fabrication of blood vessels-like models for preclinical studies of pathologies under flow conditions," Biofabrication **9**(2), 025033 (2017).
18. J. Zhang, K. Sugioka, and K. Midorikawa, "Laser-induced plasma-assisted ablation of fused quartz using the fourth harmonic of a Nd + :YAG laser," Appl. Phys. A: Mater. Sci. Process. **67**(5), 545–549 (1998).
19. J. Zhang, K. Sugioka, and K. Midorikawa, "Direct fabrication of microgratings in fused quartz by laser-induced plasma-assisted ablation with a KrF excimer laser," Opt. Lett. **23**(18), 1486 (1998).
20. C. Pan, K. Chen, B. Liu, L. Ren, J. Wang, Q. Hu, L. Liang, J. Zhou, and L. Jiang, "Fabrication of micro-texture channel on glass by laser-induced plasma-assisted ablation and chemical corrosion for microfluidic devices," J. Mater. Process. Technol. **240**, 314–323 (2017).
21. R. R. Behera and M. R. Sankar, "State of the Art on Under Liquid Laser Beam Machining," Mater. Today: Proc. **2**(4-5), 1731–1740 (2015).
22. G. Y. Mak, E. Y. Lam, and H. W. Choi, "Liquid-immersion laser micromachining of GaN grown on sapphire," Appl. Phys. A **102**(2), 441–447 (2011).
23. J. Lu, R. Q. Xu, X. Chen, Z. H. Shen, X. W. Ni, S. Y. Zhang, and C. M. Gao, "Mechanisms of laser drilling of metal plates underwater," J. Appl. Phys. **95**(8), 3890–3894 (2004).
24. X. Song, X. Q. Wu, K. L. Xiao, C. Li, H. Y. Wang, and M. Q. Jiang, "Nanosecond laser ablation of a metallic glass in water: a high time-resolved imaging study," Philos. Mag. **100**(21), 2708–2720 (2020).
25. E. Markauskas and P. Gečys, "Thin water film assisted glass ablation with a picosecond laser," Procedia CIRP **74**, 328–332 (2018).
26. R. An, Y. Li, Y. Dou, H. Yang, and Q. Gong, "Simultaneous multi-microhole drilling of soda-lime glass by water-assisted ablation with femtosecond laser pulses," Opt. Express **13**(6), 1855 (2005).
27. J. Xu, D. Wu, J. Y. Ip, K. Midorikawa, and K. Sugioka, "Vertical sidewall electrodes monolithically integrated into 3D glass microfluidic chips using water-assisted femtosecond-laser fabrication for in situ control of electrotaxis," RSC Adv. **5**(31), 24072–24080 (2015).

Optics EXPRESS

28. P. Gečys, J. Dudutis, and G. Račiukaitis, "Nanosecond Laser Processing of Soda-Lime Glass," J. Laser Micro/Nanoeng. **10**(3), 254–258 (2015).
29. N. Krstulović, S. Shannon, R. Stefanuik, and C. Fanara, "Underwater-laser drilling of aluminum," Int. J. Adv. Manuf. Technol. **69**(5-8), 1765–1773 (2013).
30. W. Charee and V. Tangwarodomnukun, "Dynamic features of bubble induced by a nanosecond pulse laser in still and flowing water," Opt. Laser Technol. **100**, 230–243 (2018).
31. Y. Hanada, K. Sugioka, I. Miyamoto, and K. Midorikawa, "Double-pulse irradiation by laser-induced plasma-assisted ablation (LIPAA) and mechanisms study," Appl. Surf. Sci. **248**(1-4), 276–280 (2005).
32. Y. Hanada, K. Sugioka, K. Obata, S. V. Garnov, I. Miyamoto, and K. Midorikawa, "Transient electron excitation in laser-induced plasma-assisted ablation of transparent materials," J. Appl. Phys. **99**(4), 043301 (2006).
33. H. Niino, Y. Kawaguchi, T. Sato, A. Narazaki, and R. Kurosaki, "Surface microstructures of silica glass by laser-induced backside wet etching," Proc. SPIE **6879**, 68790C (2008).
34. K. Zimmer, R. Böhme, M. Ehrhardt, and B. Rauschenbach, "Mechanism of backside etching of transparent materials with nanosecond UV-lasers," Appl. Phys. A **101**(2), 405–410 (2010).
35. D. Nieto, T. Delgado, and M. T. Flores-Arias, "Fabrication of microchannels on soda-lime glass substrates with a Nd:YVO_4 laser," Opt. Lasers Eng. **63**, 11–18 (2014).
36. T. Pravinraj and R. Patrikar, "Modeling and characterization of surface roughness effect on fluid flow in a polydimethylsiloxane microchannel using a fractal based lattice Boltzmann method," AIP Adv. **8**(6), 065112 (2018).
37. A. M. Ross, Z. Jiang, M. Bastmeyer, and J. Lahann, "Physical Aspects of Cell Culture Substrates: Topography, Roughness, and Elasticity," Small **8**(3), 336–355 (2012).
38. A. Bourkoula, V. Constantoudis, D. Kontziampasis, P. S. Petrou, S. E. Kakabakos, A. Tserepi, and E. Gogolides, "Roughness threshold for cell attachment and proliferation on plasma micro-nanotextured polymeric surfaces: the case of primary human skin fibroblasts and mouse immortalized 3T3 fibroblasts," J. Phys. D: Appl. Phys. **49**(30), 304002 (2016).
39. R. M. Vázquez, G. Cerullo, R. Ramponi, and R. Osellame, "Optofluidic Biochips," in *Femtosecond Laser Micromachining* (Springer, 2012), pp. 389–419.
40. A. Kruusing, "Underwater and water-assisted laser processing: Part 1—general features, steam cleaning and shock processing," Opt. Lasers Eng. **41**(2), 307–327 (2004).
41. W. Charee, V. Tangwarodomnukun, and C. Dumkum, "Laser ablation of silicon in water under different flow rates," Int. J. Adv. Manuf. Technol. **78**(1-4), 19–29 (2015).